AIP | Journal of Applied Physics

Broadband near ultra violet sensitization of 1 m luminescence in Yb3+-doped CeO2 crystal

Jumpei Ueda and Setsuhisa Tanabe

Citation: J. Appl. Phys. **110**, 073104 (2011); doi: 10.1063/1.3642984
View online: http://dx.doi.org/10.1063/1.3642984
View Table of Contents: http://jap.aip.org/resource/1/JAPIAU/v110/i7
Published by the American Institute of Physics.

Related Articles

Microcavity effects in SiGe/Si heterogeneous nanostructures prepared by electrochemical anodization of SiGe/Si multiple quantum wells
J. Appl. Phys. 110, 103101 (2011)

Microstructure, optical property, and electronic band structure of cuprous oxide thin films
J. Appl. Phys. 110, 103503 (2011)

Suppression of luminescence quenching at the nanometer scale in Gd2O3 doped with Eu3+ or Tb3+: Systematic comparison between nanometric and macroscopic samples of life-time, quantum yield, radiative and non-radiative decay rates
J. Appl. Phys. 110, 094317 (2011)

Influence of local atomic configuration in AlGdN phosphor thin films on deep ultra-violet luminescence intensity
J. Appl. Phys. 110, 093108 (2011)

Comparative investigation on the 2.7m emission in Er3+/Ho3+ codoped fluorophosphate glass
J. Appl. Phys. 110, 093106 (2011)

Additional information on J. Appl. Phys.

Journal Homepage: http://jap.aip.org/
Journal Information: http://jap.aip.org/about/about_the_journal
Top downloads: http://jap.aip.org/features/most_downloaded
Information for Authors: http://jap.aip.org/authors

ADVERTISEMENT

Downloaded 21 Nov 2011 to 130.54.110.71. Redistribution subject to AIP license or copyright; see http://jap.aip.org/about/rights_and_permissions

Broadband near ultra violet sensitization of 1 μm luminescence in Yb^{3+}-doped CeO_2 crystal

Jumpei Ueda[1,a] and Setsuhisa Tanabe[1,2]
[1]*Graduate School of Human and Environmental Studies, Kyoto University, Sakyo-ku, Kyoto 606-8501, Japan*
[2]*Japan Science and Technology Agency Precursory Research for Embryonic Science and Technology (JST-PRESTO), Chiyoda, Tokyo 102-0075, Japan*

(Received 10 August 2011; accepted 24 August 2011; published online 4 October 2011)

Broadband spectral modification of near ultra violet (UV) light to infra-red (IR) light is investigated in Yb^{3+}-doped CeO_2 polycrystalline ceramics sintered in different atmospheres (air, oxygen, and 95%N_2-5%H_2). The intense Yb^{3+} photoluminescence (PL) peaked at 970 nm was observed by the UV excitation at around 390 nm in the samples except those sintered under N_2-H_2. A broad photoluminescence excitation (PLE) band of Yb^{3+} luminescence peaked at 390 nm corresponds to the absorption band and the photocurrent excitation band in the non-doped CeO_2 crystal, which are also in accordance with the PLE band of Eu^{3+} luminescence in the Eu^{3+}-doped CeO_2. Judging from these results, the PLE band is attributed to the charge transfer (CT) band from O^{2-} to Ce^{4+}, but not to the CT from O^{2-} to Yb^{3+}. From the sintering atmosphere dependence of the PL and PLE, we found that the oxygen vacancies and Ce^{3+} impurities are not responsible for the 390 nm-absorption band but they work as a quenching center for the Yb^{3+} luminescence. © *2011 American Institute of Physics*. [doi:10.1063/1.3642984]

I. INTRODUCTION

Luminescent solar concentrating materials have attracted a great deal of interest for photovoltaic applications to improve the efficiency of solar cells by modifying the solar spectrum. The crystalline silicon (c-Si) solar cells most effectively convert photons with energy close to its semiconductor bandgap at 1.1 eV. The mismatch between the incident solar spectrum and the spectral response of the solar cells is one of the main reasons to limit the cell efficiency. The efficiency limit of the c-Si have been estimated to be 29% by Shockley and Queisser.[1] However, this limit is estimated to be improved up to 38.4% by modifying the solar spectrum by quantum cutting (downconverting) phosphors that convert one photon of high energy into two photons of lower energy.[2]

Quantum cutting conversion from a visible/UV photon shorter than 500 nm to two or more infrared photons have been reported in rare earth ions pairs of Tb^{3+}-Yb^{3+},[3] Pr^{3+}-Yb^{3+},[4,5] and Er^{3+}-Yb^{3+}.[6] The Yb^{3+} ion is suitable as an acceptor and emitter because the energy of only excited level of Yb^{3+} ($\sim$1.2 eV) is in accordance with the bandgap of c-Si ($\sim$1.1 eV) and the luminescent quantum efficiency of Yb^{3+} is mostly close to 100%. However, since absorption transitions of Pr^{3+}, Tb^{3+}, and Er^{3+} as a donor are due to the forbidden f-f transitions, the absorption line-width is mostly sharp and the absorption cross-section is not large. In order to overcome this problem, the allowed f-d transitions of Ce^{3+} (Refs. 7–11) and Eu^{2+} (Refs. 12–14) or the host absorptions of ZnO crystals[15] are considered to be used as the sensitizer of Yb^{3+} luminescence in order to absorb the solar spectrum efficiently.

In this study, we focused on the host absorption of CeO_2 crystals. The CeO_2 crystals have a bandgap of 3.2 eV between the occupied 2p band of O and the narrow 4f band of Ce, and another wider bandgap of 6 eV between the 2p band of O and the band of 5d and 6s states of Ce.[16–18] There is a possibility that the CeO_2 crystals can be used as near UV sensitizer of luminescence of trivalent rare earth ions because of the former band absorption, which is attributed to the charge transfer (CT) from O^{2-} to Ce^{4+}. In addition, trivalent rare earth ions can be introduced easily into the CeO_2 crystals due to their close ionic radius to that of Ce^{4+} ion compared with other metal oxide hosts, such as ZnO and TiO_2, which also have an absorption band in the near UV range. Therefore, Yb^{3+}-doped CeO_2 crystals can be a good candidate as the wavelength converter of near UV photons to IR photons. Although the energy transfer from the host absorption to the rare earth ions in the CeO_2 crystals doped with Eu^{3+} and Sm^{3+} have been reported,[19–23] these optical properties of Yb^{3+}-doped CeO_2 have never been studied. In addition, even non-doped CeO_2 crystals can easily create Ce^{3+} ions in the lattice by formation of the oxygen vacancies under some reducing conditions. In order to distinguish the near UV absorption band by the CT transition from O^{2-} to Ce^{4+} from those by the oxygen vacancies and Ce^{3+}/Yb^{3+} impurities, we investigated the optical properties of the CeO_2 crystals doped with various concentrations of Yb^{3+} prepared under oxidizing and reducing atmosphere.

II. EXPERIMENTAL PROCEDURE

Polycrystalline ceramics with the compositions of (100-x) CeO_2-x Yb_2O_3 (x = 0, 0.05, 0.1, 0.5, 1, 3, 5, 10) in mol % were prepared by the solid-state reaction. Powders of CeO_2 (99.99%) and Yb_2O_3 (99.99%) were used as starting materials. The powders were mixed well in an alumina

[a]Author to whom correspondence should be addressed. Electronic mail: j.ueda@at3.ecs.kyoto-u.ac.jp.

 © 2011 American Institute of Physics

Downloaded 21 Nov 2011 to 130.54.110.71. Redistribution subject to AIP license or copyright; see http://jap.aip.org/about/rights_and_permissions

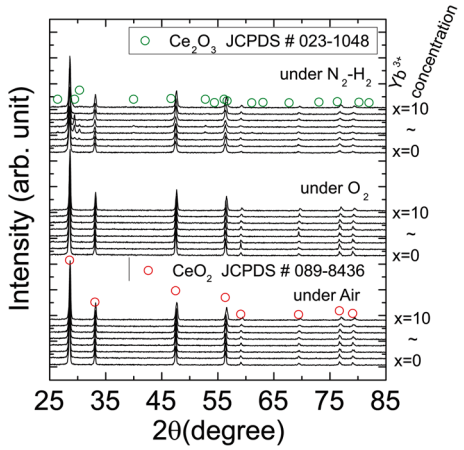

FIG. 1. (Color online) XRD patterns of samples sintered under air, O_2 and N_2-H_2 atmosphere with various Yb^{3+} concentrations (x = 0, 0.05, 0.1, 0.5, 1, 3, 5, 10).

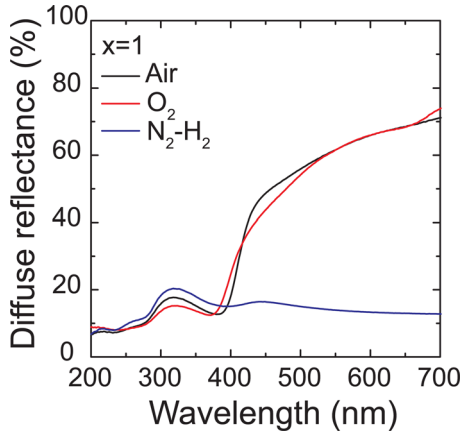

FIG. 2. (Color online) Diffuse reflectance spectra of samples sintered under various atmospheres with 1 mol % Yb_2O_3.

mortar and pressed into a pellet of 10 mm diameter. The obtained pellets were sintered at 1600 °C for 6 h under air, O_2, and N_2-H_2 (5%) atmospheres. The final products were identified by an x-ray diffraction (XRD) measurement (Rigaku, UltimaIV). In addition, in order to evaluate the lattice constants of the crystals correctly, MgO powders (30 wt. %) were mixed into the obtained sample powders as a reference of the angle correction. The photoluminescence (PL) spectra by a 378 nm laser diode (LD) (Nichia, NDHU110A-PAE3) excitation were measured by combining a monochromator (Nikon, G250) and a Si photodiode (Electro-Optical System, Inc., S-025-H). For the PLE spectra measurement, the samples were excited by monochromatic light obtained by combining a Xe lamp (Asahi Spectra Co., Ltd., MAX-302) and the monochromator. The Yb^{3+} luminescence was detected by combining a bandpass filter (1000 nm) and the Si photodiode. All the obtained PL and PLE spectra were calibrated by a standard halogen lamp (Labsphere, SCL-600) and a standard Si photodiode (Hamamatsu Photonics, S1337-1010BQ) for the precise photometry. For measurement of the photocurrent excitation (PCE) spectrum, gold electrodes were deposited on the sample which was partially masked by a tape of 1 mm width in order to separate the electrodes. The sample connected with two nickel wires was mounted into a vacuum chamber in order to suppress surface current of the sample. The sample was excited by a combination of the Xe lamp and the monochromator. A direct voltage of 30 V was applied to the sample and photocurrents were measured with a digital electrometer (ADVANTEST 8240).

III. RESULTS

A. XRD patterns

Figure 1 shows XRD patterns of the obtained samples doped with various Yb^{3+} concentrations sintered under various conditions. The XRD patterns of the samples sintered under air and O_2 correspond well to the reference data of the CeO_2 crystal (JCPDS No. 89-8436) as a single phase, while some samples sintered under N_2-H_2 also contain weak diffraction patterns of Ce_2O_3 (JCPDS No. 023-1048).

B. Optical properties (diffuse reflectance, PL and PLE spectra)

The colors of the obtained samples sintered under air and O_2 were light yellow at any Yb^{3+} concentration while those sintered under N_2-H_2 were deep black. Figure 2 shows the diffuse reflectance spectra of the CeO_2:Yb^{3+} (x = 1; air, O_2, and N_2-H_2). An absorption band was observed in the range between 300 and 450 nm in all the samples. This band can be attributed to the CT band from O^{2-} to Ce^{4+}. In addition, a broad and strong absorption band was observed over visible range in the CeO_2:Yb^{3+} (x = 1; N_2-H_2). This broad absorption band is a cause of the black color of the samples sintered under N_2-H_2. Figure 3 shows the diffuse reflectance spectra of the CeO_2:Yb^{3+} (x = 0–10; air). The onset absorption wavelengths were red-shifted from 430–460 nm with increasing Yb^{3+} concentration. The intensity of the absorption band was not significantly changed by Yb^{3+} concentration.

Figure 4 shows the PL spectra of the CeO_2:Yb^{3+} (x = 0.5; air, O_2 and N_2-H_2) by the 378 nm excitation. The intense luminescence band at around 970 nm was observed

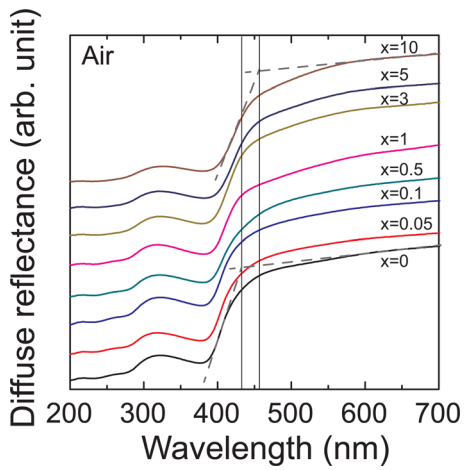

FIG. 3. (Color online) Diffuse reflectance spectra of the samples sintered under air with various Yb^{3+} concentrations.

Downloaded 21 Nov 2011 to 130.54.110.71. Redistribution subject to AIP license or copyright; see http://jap.aip.org/about/rights_and_permissions

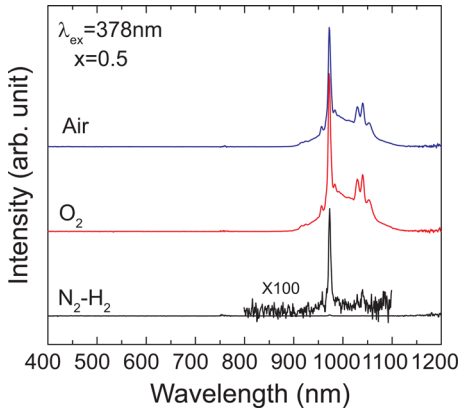

FIG. 4. (Color online) PL spectra by 378 nm excitation in the samples sintered under air, O_2, and N_2-H_2 with Yb^{3+} (0.5 mol %).

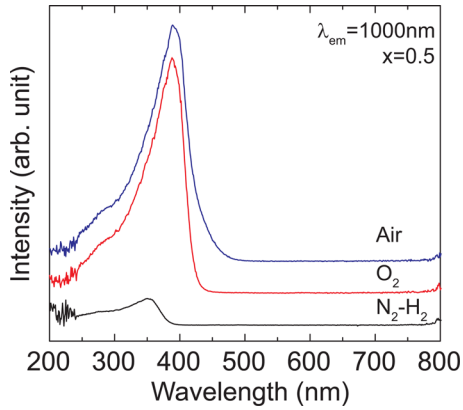

FIG. 6. (Color online) PLE spectra monitoring 1000 nm luminescence of the samples sintered under air, O_2, and N_2-H_2 with Yb^{3+} (0.5 mol %).

in the CeO_2:Yb^{3+} sintered under air and O_2. This band is attributed to the Yb^{3+}:$^2F_{5/2} \rightarrow {}^2F_{7/2}$ transition. Although luminescence intensity was weak, the Yb^{3+} luminescent band was also observed in the CeO_2:Yb^{3+} sintered under N_2-H_2. Figure 5 shows the PL spectra of the CeO_2:Yb^{3+} (x = 0–10; air). The Yb^{3+} luminescence was observed in all the samples doped with Yb^{3+} and the luminescent intensity once increased at first and decreased with increasing Yb^{3+} concentration. In addition, the spectral shape of the Yb^{3+} luminescence changed with Yb^{3+} concentration.

Figure 6 shows the PLE spectra monitoring the Yb^{3+} luminescence in the CeO_2:Yb^{3+} (x = 0.5; air, O_2, and N_2-H_2). The PLE band was observed in range between 200 and 450 nm in all the samples, which can be attributed to the CT transition from O^{2-} to Ce^{4+}. The PLE intensities in the samples sintered under air and O_2 were much stronger than those sintered under N_2-H_2. In addition, the PLE peak wavelengths were different in the samples sintered under various atmospheres. The PLE peak wavelength at about 350 nm in the sample sintered under N_2-H_2 was shorter than that at 390 nm in the samples sintered under air and O_2. Figure 7 shows the PLE spectra monitoring the Yb^{3+} luminescence in the samples sintered under air with various Yb^{3+} concentrations. The PLE peak intensities and wavelengths were changed with increasing Yb^{3+} concentration.

Figure 8 shows the photocurrent excitation spectra of the CeO_2:Yb^{3+} (x = 0 and 0.1; air) and the PLE spectrum of the CeO_2:Yb^{3+} (x = 0.1; air). The PCE band was observed at 385 and 388 nm in the pure CeO_2 and CeO_2:Yb^{3+} (x = 0.1; air) at room temperature, respectively. The PCE peak wavelength corresponds to the PLE peak wavelength in the CeO_2:Yb^{3+} (x = 0.1; air). This PCE band can also be attributed to the CT transfer from O^{2-} to Ce^{4+}. Figure 9 shows the PLE spectra of CeO_2:Eu^{3+} monitoring the Eu^{3+}:$^5D_0 \rightarrow {}^7F_1$ luminescence and CeO_2:Yb^{3+} (x = 1; air) monitoring the Yb^{3+}:$^2F_{5/2} \rightarrow {}^2F_{7/2}$ luminescence. The PLE peak wavelength at 387 nm in the CeO_2:Eu^{3+} is in accordance with that at 389 nm in the CeO_2:Yb^{3+}.

IV. DISCUSSION

A. Substitution of Yb^{3+} for Ce^{4+} site

Lattice constants of the CeO_2:Yb^{3+} crystals with cubic symmetry were estimated from XRD results. Figure 10 shows the Yb^{3+} concentration dependence of the lattice constant in the samples sintered under air, O_2, and N_2-H_2. The lattice constants of the samples sintered under any atmosphere decreased with increasing Yb^{3+} concentration. In addition, the lattice constants of the samples sintered under N_2-H_2 were larger than that under air and O_2 at any Yb^{3+}

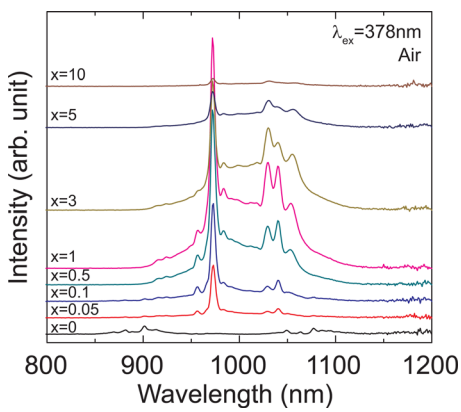

FIG. 5. (Color online) PL spectra by 378 nm excitation of the samples sintered under air with various Yb^{3+} concentrations.

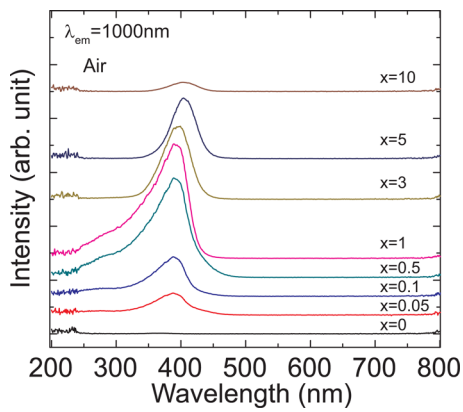

FIG. 7. (Color online) PLE spectra monitoring 1000 nm luminescence of the samples sintered under air with various Yb^{3+} concentrations.

Downloaded 21 Nov 2011 to 130.54.110.71. Redistribution subject to AIP license or copyright; see http://jap.aip.org/about/rights_and_permissions

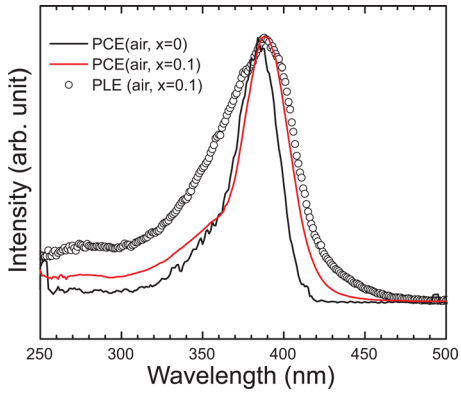

FIG. 8. (Color online) Photocurrent excitation spectrum of pure CeO_2 sample sintered under air and PLE spectrum of samples sintered under air with Yb^{3+} concentration (0.1 mol %).

concentration. These changes of the lattice constants can be caused by formation of some defects in the CeO_2-based crystals. The possible defect reactions are (1) Ce^{3+} formation in CeO_2 crystals and (2) incorporation of Yb^{3+} impurities into the CeO_2 crystals, which can be described by

$$2CeO_2 \rightarrow 2Ce'_{Ce} + 3O_o^x + V_O^{\cdot\cdot} + 1/2O_2, \quad (1)$$

$$Yb_2O_3 \rightarrow 2Yb'_{Ce} + 3O_o^x + V_O^{\cdot\cdot}, \quad (2)$$

respectively. The ionic radii of Ce^{3+}, Yb^{3+}, and Ce^{4+} at 8-hold coordination are described in the order of Ce^{3+} (1.143 Å), Yb^{3+} (0.985 Å) and Ce^{4+} (0.97 Å).[24] Therefore, the lattice expansion of the CeO_2:Yb^{3+} crystals sintered under N_2-H_2 can be explained by the substitution smaller Ce^{4+} ion site with much larger Ce^{3+} ion. However, the lattice shrink of Yb^{3+}-doped CeO_2 with increasing Yb^{3+} concentration is not explained by the ionic radius in all the samples because the ionic radii of Yb^{3+} and Ce^{4+} are almost the same. Therefore, the lattice shrink can be caused by formation of oxygen vacancies, $V_O^{\cdot\cdot}$ in Eq. (2). The lattice shrink of $Ce_{1-x}Ln_xO_{2-x}$ (Ln = Yb,Lu) with increasing Yb or Lu concentration caused by oxygen vacancies have been reported by Małgorzata *et al.*[25] The Yb^{3+} dependence of the lattice constant in the reference data are in good agreement with our results.

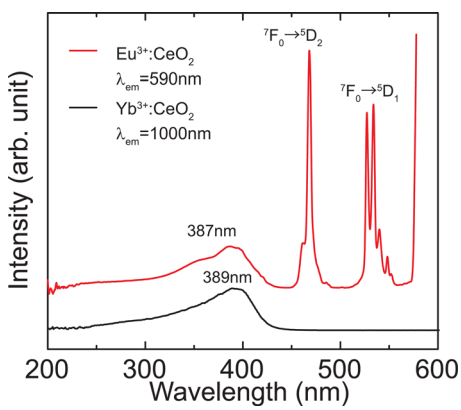

FIG. 9. (Color online) PLE spectra of CeO_2:Eu^{3+} (1 mol %) sintered under air monitoring Eu^{3+} luminescence at 590 nm and that of CeO_2:Yb^{3+} (x = 1) sintered under air monitoring Yb^{3+} luminescence at 1000 nm.

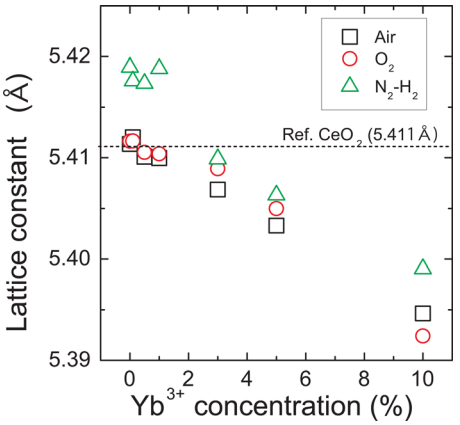

FIG. 10. (Color online) Yb^{3+} concentration dependence of lattice constant in samples sintered under air, O_2, and N_2-H_2.

B. Crystal structure and photoluminescence property

Figure 11 shows the PL spectra by 378 nm excitation normalized by the peak intensity at 978 nm in the sample sintered under air. With increase of Yb^{3+} concentration, the bandwidth was broadened and the PL intensity ratio between 1030 and 1040 nm peaks was changed. The observed broadening of the Yb^{3+} luminescence can be interpreted from the viewpoint of the inhomogeneity in the local environment around Yb^{3+} caused by the substitution by itself. As discussed in the previous section, the substitution of Yb^{3+} introduces oxygen vacancies in the samples for the requirement of stoichiometry and charge neutrality. Figure 12 shows a possible site variations of Yb^{3+} in the Yb:CeO_2 crystal. In this figure, the cube shows the anion polyhedron surrounding a cation. Assuming that the first-nearest eight sites of Yb^{3+} are occupied by oxygen ions and one oxygen vacancies at most and the second-nearest twelve sites would be occupied by the Ce^{4+} ions and one Yb^{3+} ion at most, there are six variations of the coordination environments around Yb^{3+}. Actually, the oxygen vacancies at the first-nearest sites and the Yb^{3+} ions at the second-nearest sites should increase with increasing Yb^{3+} concentration. Therefore, the inhomogeneity of the Yb^{3+} sites also increases with increasing Yb^{3+} concentration, which contributes to the broadening of Yb^{3+} luminescence spectra. In addition, the change of local coordination of the

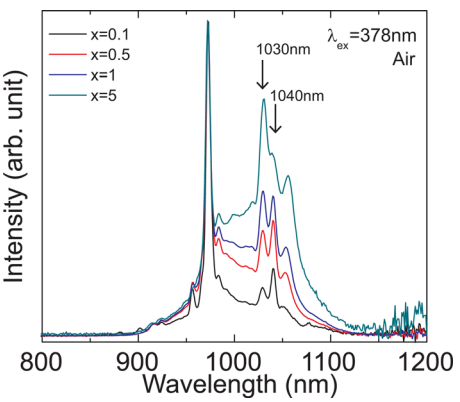

FIG. 11. (Color online) Normalized PL spectra at 970 nm peak by 378 nm excitation in the samples sintered under air with various Yb^{3+} concentrations.

Downloaded 21 Nov 2011 to 130.54.110.71. Redistribution subject to AIP license or copyright; see http://jap.aip.org/about/rights_and_permissions

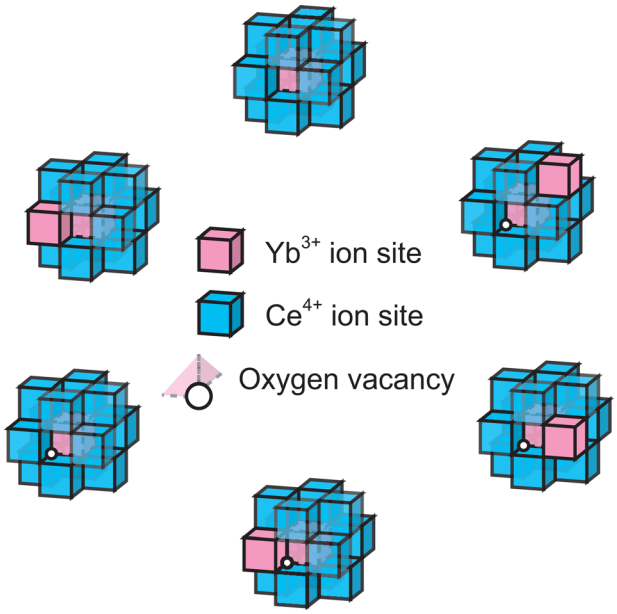

FIG. 12. (Color online) Site variation of Yb^{3+} ion with one oxygen vacancy at the first-nearest neighbors and another Yb^{3+} ion at the second-nearest sites.

Yb^{3+} ion with Yb^{3+} concentration can also lead to variation of the spectral shape of the Yb^{3+} luminescence.

C. Optimum sintering atmosphere and Yb^{3+} concentration for 1 μm luminescence

The PL and PLE intensity in the CeO_2:Yb^{3+} sintered under N_2-H_2 was much lower than those sintered under air and O_2. Therefore, the PLE band at around 390 nm cannot be due to the oxygen vacancies and the 4f-5d transition of Ce^{3+} because in these samples sintered under N_2-H_2, concentration of Ce^{3+} impurities and oxygen vacancies are the highest. These results rather indicate that the Ce^{3+} impurities and/or oxygen vacancies can work as a quenching center of the Yb^{3+} luminescence in CeO_2 crystals. In addition, another important point to be addressed is transparency of the samples for optimum use as a wavelength convertor of the solar spectrum. Although the CeO_2:Yb^{3+} crystals sintered under air and O_2 show the intense Yb^{3+} luminescence, they are not completely transparent in the present stage. Because of cubic symmetry, the fluorite type crystals can be fabricated into transparent ceramics by some appropriate methods such as sintering of nano powders in vacuum or hot isostatic pressing (HIP) process of nano powders. However, the sintering of the samples under vacuum cannot avoid the formation of the Ce^{3+} impurities and oxygen vacancies in the crystals. Therefore, efficient downconvertors of the CeO_2:Yb^{3+} transparent ceramics with less amount of such quenching centers can be obtained by post-annealing under O_2 after sintering in vacuum or the HIP process.

Figure 13 shows the Yb^{3+} concentration dependence of the PL intensity by the 378 nm excitation in the samples sintered under air. With increasing Yb^{3+} concentration, the PL intensity increased until about 1 mol % of Yb_2O_3, and then decreased; i.e., the concentration quenching of Yb^{3+} luminescence occurs above 1 mol % Yb_2O_3. Therefore, we conclude that optimum Yb^{3+} concentration is between 0.5 and 1 mol %.

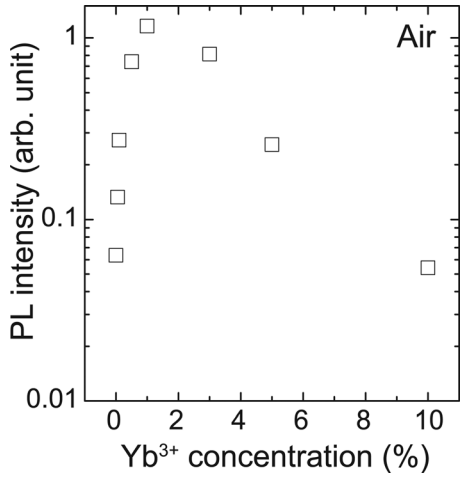

FIG. 13. Yb^{3+} concentration dependence of PL intensity by 378 nm excitation in samples sintered under air.

D. Assignment of UV-band

The absorption band in the diffuse reflectance spectra and PLE/PCE bands at around 390 nm were attributed to the charge transfer (CT) transition from O^{2-} to Ce^{4+} in this study because the band wavelength corresponds to the bandgap (Eg = 3.2 eV) attributed to $2p(O) \rightarrow 4f(Ce)$,[17,18] which is exactly equivalent to the charge transfer from O^{2-} to Ce^{4+}. However, in the CeO_2:Eu^{3+} crystals prepared by the sol-gel method, the shorter CT band from O^{2-} to Ce^{4+} at 350 nm has been reported.[19,20,22,23] The difference of the CT band energy between the CeO_2:Yb^{3+} bulk prepared by the solid-state reaction and the reported CeO_2:Eu^{3+} powders prepared by sol-gel method can be caused by the way of preparation and the sintering temperature. In general, the CeO_2 powders prepared by sol-gel method have a few tenths nm in the crystallite size. In this case, the quantum size effect cannot be ignored and the CT energy gap would be blue-shifted. Actually, the CeO_2:Eu^{3+} prepared by the solid state reaction at 1360 °C has the longer PLE band ($\lambda = 373$ nm).[21] Li *et al*. have reported that with increasing temperature of annealing in the CeO_2:Eu^{3+} prepared by the sol-gel method the lattice constant increases and also the CT band is red-shifted. Therefore, the band structure of CeO_2 can be very sensitive to the crystallite size and the lattice constant. In the CeO_2:Eu^{3+} prepared by our sintering process, the PLE peak has longer wavelength at 387 nm rather than those in CeO_2:Eu^{3+} mentioned above and good accordance with the PLE peak at 389 nm in the CeO_2:Yb^{3+}. This result also supports our conclusion that the PLE band at around 390 nm is the CT band from O^{2-} to Ce^{4+}, independent of the doped lanthanide ions.

Figure 14 shows the PLE peak wavelengths as a function of the lattice constant in the CeO_2:Yb^{3+} (air). The PLE peak wavelengths were red-shifted with decreasing lattice constant. Generally, the lattice constant of a solid is directly correlated with its energy band structure, so that the shift of

Downloaded 21 Nov 2011 to 130.54.110.71. Redistribution subject to AIP license or copyright; see http://jap.aip.org/about/rights_and_permissions

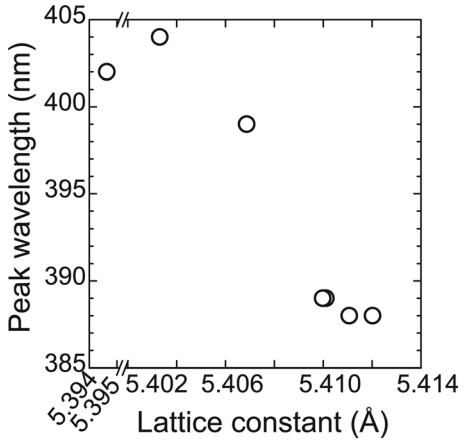

FIG. 14. PLE peak wavelengths as a function of lattice constant in samples sintered under air.

the PLE band can be explained by the CT band. In addition, the PCE band at 385 nm was observed in the pure CeO_2. The photocurrent can be caused by the electron transfer between the Ce^{4+} and the photoinduced Ce^{3+} because the electronic conductivity in the CeO_2 crystal due to existence of Ce^{3+}/Ce^{4+} has been reported.[26] Therefore, this PCE band is attributed to the CT transition from O^{2-} to Ce^{4+}, but not to the CT transition from O^{2-} to Yb^{3+}. The results of the lattice constant dependence of the PLE peak and the photocurrent excitation spectra also support that the observed PLE band at 390 nm is due to CT transition from O^{2-} to Ce^{4+}. However, in the samples doped with low concentration of Yb_2O_3 (<1 mol %), both PLE and PCE spectra have a small edge in shorter wavelength side of the peak. This edge structure in the PLE and PCE spectra was not observed in the pure CeO_2. Therefore, the PLE and PCE edges in the samples doped with low concentration of Yb_2O_3 can be attributed to the CT transition from O^{2-} to Yb^{3+}.

E. Energy transfer mechanisms

The Yb^{3+} ion has only one 4f excited level at around 1 μm, so that there is no spectral overlap between the absorption band (380 nm) of CeO_2 and that of Yb^{3+}. Therefore, the resonant energy transfer by the multipolar interaction and exchange interaction are not likely to occur. One possibility is an energy transfer by the quantum cutting mechanism. For instance, although Tb^{3+} ion does not have the energy level at around 1 μm, the combination of one Tb^{3+} and two Yb^{3+} ions shows the energy transfer by the quantum cutting from Tb^{3+}:$^5D_4$ (480 nm) to Yb^{3+}:$^2F_{5/2}$ (1000 nm).[3] Thus, although the CeO_2 crystal does not either have an intermediate level at 1 μm, the quantum cutting in the CeO_2:Yb^{3+} may occur through the same process, i.e., conversion of a UV photon into two or three infrared photons (see Fig. 15). On the other hand, the photo-induced current was observed by photoconductivity measurement. In this process, the electrons may be caught by Yb^{3+} with some activation energy. This electron trap by the Yb^{3+} ion results in formation of the Yb^{2+} ion and the positive hole. This situation is similar to the charge transfer state from O^{2-} to Yb^{3+}. The energy transfer from the CT state ($O^{2-} + h^+ - Yb^{2+}$) to the $^2F_{5/2}$ level of Yb^{3+} by the radiative and non-radiative process has been reported in many crystals.[27–29] Therefore, another possibility is an energy transfer through the CT state. In order to determine the detailed energy transfer mechanisms and possibility of quantum cutting, further experiments are necessary.

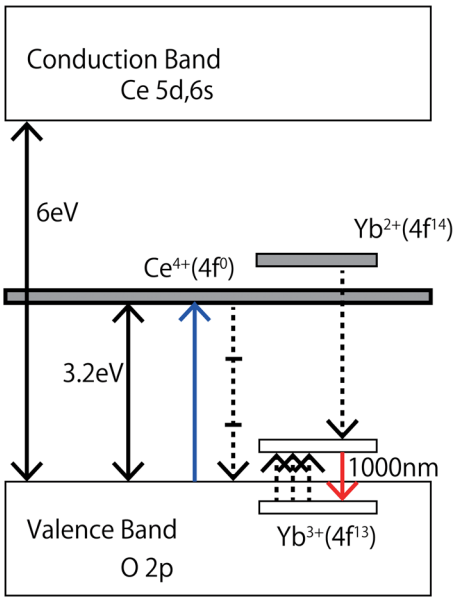

FIG. 15. (Color online) Energy level diagram of CeO_2:Yb^{3+}. Quantum cutting process from one photon to two or three photons is energetically possible.

V. CONCLUSION

The intense 1 μm luminescence band attributed to the Yb^{3+}: $^2F_{5/2} - {}^2F_{7/2}$ transition was obtained by the UV excitation at around 390 nm in the CeO_2:0.5 ~1 mol %Yb^{3+} sintered under air and O_2 with various Yb^{3+} concentrations. The broad PLE band of Yb^{3+} luminescence peaked at 390 nm corresponds to the absorption band and the PCE band in non-doped CeO_2 crystal, which are also in accordance with the PLE band of Eu^{3+} luminescence in the Eu^{3+}-doped CeO_2. Therefore, we conclude that PLE band is due to the CT band from O^{2-} to Ce^{4+}, neither to that from O^{2-} to Yb^{3+}, the oxygen vacancies nor to Ce^{3+} impurities. Since these crystals are transparent in wide wavelength region above 400 nm and convert near UV photon into 1 μm photons, an application to a downconverting phosphor for solar cells can be feasible.

ACKNOWLEDGMENTS

This work was supported by Japan Science and Technology Agency - Precursory Research for Embryonic Science and Technology (JST-PRESTO), a Grant-in-Aid for Scientific Research from Japan Society for the Promotion (Grant No. 22-2797) and Grant-in Aid for Scientific Research(B) (Grant No. 23350099).

[1]W. Shockley and H. J. Queisser, J. Appl. Phys. **32**, 510 (1961).
[2]T. Trupke, M. A. Green, and P. Wurfel, J. Appl. Phys. **92**, 1668 (2002).

Downloaded 21 Nov 2011 to 130.54.110.71. Redistribution subject to AIP license or copyright; see http://jap.aip.org/about/rights_and_permissions

[3]P. Vergeer, T. J. H. Vlugt, M. H. F. Kox, M. I. Den Hertog, J. P. J. M. Van Der Herden, and A. Meijerink, Phys. Rev. B **71**, 014119 (2005).
[4]B. M. van der Ende, L. Aarts, and A. Meijerink, Adv. Mater. **21**, 3073 (2009).
[5]Y. Katayama and S. Tanabe, Materials **3**, 2405 (2010).
[6]J. J. Eilers, D. Biner, J. T. Van Wijngaarden, K. Krämer, H. U. Güdel, and A. Meijerink, Appl. Phys. Lett. **96**, 151106 (2010).
[7]D. Chen, Y. Wang, Y. Yu, P. Huang, and F. Weng, J. Appl. Phys. **104**, 116105 (2008).
[8]J. Ueda and S. Tanabe, J. Appl. Phys. **106**, 043101 (2009).
[9]Q. Zhang, J. Wang, G. Zhang, and Q. Su, J. Mater. Chem. **19**, 7088 (2009).
[10]J. Chen, H. Guo, Z. Li, H. Zhang, and Y. Zhuang, Opt. Mater. **32**, 998 (2010).
[11]H. Lin, S. Zhou, H. Teng, Y. Li, W. Li, X. Hou, and T. Jia, J. Appl. Phys. **107**, 043107 (2010).
[12]J. Zhou, Y. Teng, G. Lin, X. Xu, Z. Ma, and J. Qiu, J. Electrochem. Soc. **157**, B1146 (2010).
[13]Y. Teng, J. Zhou, S. Ye, and J. Qiu, J. Electrochem. Soc. **157**, A1073 (2010).
[14]H. Lin, D. Chen, Y. Yu, Z. Shan, P. Huang, A. Yang, and Y. Wang, J. Alloys Compd. **509**, 3363 (2011).
[15]S. Ye, N. Jiang, F. He, X. Liu, B. Zhu, Y. Teng, and J. R. Qiu, Opt. Express **18**, 639 (2010).
[16]N. V. Skorodumova, R. Ahuja, S. I. Simak, I. A. Abrikosov, B. Johansson, and B. I. Lundqvist, Phys. Rev. B **64**, 115108 (2001).
[17]Z. C. Orel and B. Orel, Phys. Status Solidi B **186**, K33 (1994).
[18]F. Marabelli and P. Wachter, Phys. Rev. B **36**, 1238 (1987).
[19]S. Fujihara and M. Oikawa, J. Appl. Phys. **95**, 8002 (2004).
[20]M. Oikawa and S. Fujihara, J. Eur. Ceram. Soc. **25**, 2921 (2005).
[21]X. Liu, S. Chen, and X. Wang, J. Lumin. **127**, 650 (2007).
[22]H. Guo and Y. Qiao, Appl. Surf. Sci. **254**, 1961 (2008).
[23]L. Li, H. K. Yang, B. K. Moon, Z. Fu, C. Guo, J. H. Jeong, S. S. Yi, K. Jang, and H. S. Lee, J. Phys. Chem. C **113**, 610 (2009).
[24]R. Shannon, Acta Crystallogr. Sec. A **32**, 751 (1976).
[25]M. A. Małgorzata, U. Burkhardt, D. Kaczorowski, M. P. Schmidt, D. Goran, and L. Kêpiánski, J. Nanopart. Res. **11**, 2113 (2009).
[26]H. L. Tuller and A. S. Nowick, J. Electrochem. Soc. **122**, 255 (1975).
[27]E. Nakazawa, Chem. Phys. Lett. **56**, 161 (1978).
[28]E. Nakazawa, J. Lumin. **18–19**, 272 (1979).
[29]I. Kamenskikh, C. Dujardin, N. Garnier, N. Guerassimova, G. Ledoux, V. Mikhailin, C. Pedrini, A. Petrosyan, and A. Vasil'ev, J. Phys. Condens. Matter **17**, 5587 (2005).

Downloaded 21 Nov 2011 to 130.54.110.71. Redistribution subject to AIP license or copyright; see http://jap.aip.org/about/rights_and_permissions